BIOCHEMISTRY
including biophysical chemistry & molecular biology

Article

pubs.acs.org/biochemistry

Investigating the Role of Zinc and Copper Binding Motifs of Trafficking Sites in the Cyanobacterium *Synechocystis* PCC 6803

Adriana Badarau, Arnaud Baslé, Susan J. Firbank, and Christopher Dennison*

Institute for Cell and Molecular Biosciences, Medical School, Newcastle University, Newcastle upon Tyne, NE2 4HH, United Kingdom

Supporting Information

ABSTRACT: Although zinc and copper are required by proteins with very different functions, these metals can be delivered to cellular locations by homologous metal transporters within the same organism, as demonstrated by the cyanobacterial (*Synechocystis* PCC 6803) zinc exporter ZiaA and thylakoidal copper importer PacS. The N-terminal metal-binding domains of these transporters ($ZiaA_N$ and $PacS_N$, respectively) have related ferredoxin folds also found in the metallochaperone Atx1, which delivers copper to PacS, but differ in the residues found in their M/IXCXXC metal-binding motifs. To investigate the role of the nonconserved residues in this region on metal binding, the sequence from $ZiaA_N$ has been introduced into Atx1 and $PacS_N$, and the motifs of Atx1 and $PacS_N$ swapped. The motif sequence can tune Cu(I) affinity only approximately 3-fold. However, the introduction of the $ZiaA_N$ motif (MDCTSC) dramatically increases the Zn(II) affinity of both Atx1 and $PacS_N$ by up to 2 orders of magnitude. The Atx1 mutant with the $ZiaA_N$ motif crystallizes as a side-to-side homodimer very similar to that found for $[Cu(I)_2{-}Atx1]_2$ (Badarau et al. *Biochemistry* 2010, *49*, 7798). In a crystal structure of the $PacS_N$ mutant possessing the $ZiaA_N$ motif ($PacS_N^{ZiaA_N}$), the Asp residue from the metal-binding motif coordinates Zn(II). This demonstrates that the increased Zn(II) affinity of this variant and the high Zn(II) affinity of $ZiaA_N$ are due to the ability of the carboxylate to ligate this metal ion. Comparison of the Zn(II) sites in $PacS_N^{ZiaA_N}$ structures provides additional insight into Zn(II) trafficking in cyanobacteria.

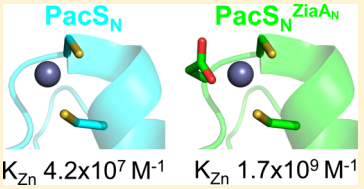

Zinc and copper are essential metal ions for most organisms but exhibit a number of important differences. The biological functions of copper primarily utilize its redox activity, which contributes to the toxicity of this metal.[1] Redox-inactive zinc is more abundant in biological systems and is required by many more proteins.[2] The tight binding of zinc and copper to biological metal sites means that the intracellular availability of both has to be carefully controlled.[3] Copper trafficking generally involves metallochaperones that deliver the metal to specific targets by ligand-exchange reactions.[3,4] No zinc metallochaperone is currently known,[5] although metallothioneins involved in zinc storage have been proposed to also act as a direct source of zinc for target proteins.[6,7]

Zinc export from the cytosol of the cyanobacterium *Synechocystis* PCC 6803 occurs via the P-type ATPase ZiaA.[8] In the same organism, the P-type ATPase PacS, along with the copper metallochaperone Atx1, traffic copper to the thylakoids for photosynthesis and respiration.[9,10] ZiaA and PacS each possess a single N-terminal metal-binding domain (MBD; $ZiaA_N$ and $PacS_N$ respectively) structurally similar to Atx1 in having a M/IXCXXC metal-binding motif anchored on a ferredoxin ($\beta\alpha\beta\beta\alpha\beta$) fold (Figure 1).[11−13] $ZiaA_N$ is unusual in having an unstructured C-terminal extension that contains seven His residues that are involved in Zn(II) binding.[13] We have recently shown that the Zn(II) affinity of $ZiaA_N$ is up to 2 orders of magnitude higher than those of $PacS_N$ and Atx1.[14] The Cu(I) affinities of copper and zinc trafficking proteins in *Synechocystis* all fall within approximately 1 order of magnitude at pH 7.0.[14] However, the Cu(I) affinity of *Synechocystis* Atx1 is almost 10-fold greater than that of $PacS_N$ (and $ZiaA_N$), and this Atx1 can dimerize in the presence of Cu(I),[11,12] which enhances its Cu(I) affinity.[14] The Cu(I) affinities of the trafficking sites are at least 6 orders of magnitude greater than their Zn(II) affinities,[14] consistent with theoretical studies,[15] yet Atx1 has been proposed to be able to bind zinc in vivo.[16]

The non-Cys residues in the M/IXCXXC motifs of metal-trafficking proteins have been implicated in metal binding and transfer.[17−22] This includes contributing to Zn(II) coordination in a Zn(II)-transporting ATPase form *Escherichia coli* (*E. coli*), facilitating the rate and extent of dissociation of the Atx1−Cu(I)−BCA complex [BCA (bicinchoninic acid) is a tight Cu(I) ligand used as a copper-transfer partner mimic], influencing the flexibility of this part of the protein, and forming potentially important hydrogen-bonds, particularly with the Cys ligands. In this work, we use the *Synechocystis* system to help understand the importance of the non-Cys residues in M/IXCXXC motifs on the binding of zinc and copper. We have grafted the motif from $ZiaA_N$ onto both Atx1 ($Atx1^{ZiaA_N}$) and $PacS_N$ ($PacS_N^{ZiaA_N}$) and have swapped these regions between Atx1 and $PacS_N$, giving $Atx1^{PacS_N}$ and $PacS_N^{Atx1}$, respectively (Figure 1C). These mutations have a limited effect (maximum ~3-fold) on Cu(I) affinity. However, introducing the $ZiaA_N$ loop has a dramatic influence on the

Received: April 19, 2013
Revised: August 14, 2013
Published: September 19, 2013

   dx.doi.org/10.1021/bi400492t | *Biochemistry* 2013, 52, 6816−6823

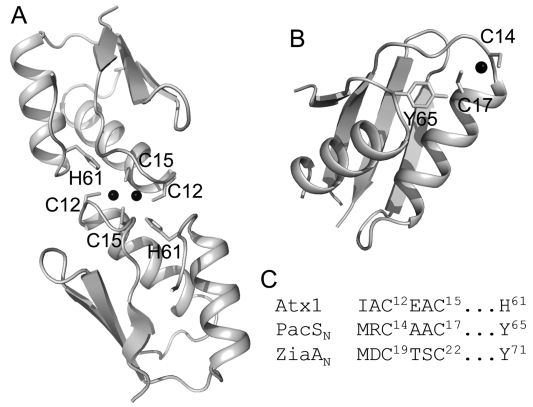

Figure 1. (A) Structure of the head-to-head dimer of Cu(I)−Atx1,[12] which is also dimeric in solution.[11,12] The Cu(I) ions are coordinated by Cys12 and Cys15 from one monomer and Cys15 from the adjacent chain. The loop 5 His61 residue hydrogen bonds with Cys15 from the same chain and with Cys12 across the dimer interface. (B) Structure of $PacS_N$ with Cu(I) coordinated by Cys14 and Cys17, with the loop 5 Tyr65 residue hydrogen bonding to Cys17.[12] The sequences of the copper binding motifs and the loop 5 residue in Atx1, $PacS_N$, and $ZiaA_N$ are compared in (C). The Atx1 variants in which the MXCXXC motifs from $PacS_N$ and $ZiaA_N$ have been introduced are called $Atx1^{PacS_N}$ (MRCAAC motif) and $Atx1^{ZiaA_N}$ (MDCTSC motif), whereas the $PacS_N$ variants possessing the Atx1 and $ZiaA_N$ M/IXCXXC sequences are referred to as $PacS_N{}^{Atx1}$ (IACEAC motif) and $PacS_N{}^{ZiaA_N}$ (MDCTSC motif). In all of these variants, the loop 5 residue has not been changed.

Zn(II) affinities of both Atx1 and $PacS_N$. In its crystal structure, Zn(II)−$Atx1^{ZiaA_N}$ forms a side-to-side dimer with the monomers bridged by a single Zn(II) ion. The introduced Asp11 residue on the $MDC^{12}TSC^{15}$ motif is involved in an intermolecular hydrogen bond with Ser14 from the adjacent molecule. In a crystal structure of Zn(II)−$PacS_N{}^{ZiaA_N}$, the metal ion is coordinated by the carboxylate of the corresponding Asp residue, which must be the cause of the enhanced Zn(II) affinity. The comparison of Zn(II)−$PacS_N{}^{ZiaA_N}$ crystal structures provide additional insight into potential intermediate sites formed during Zn(II) trafficking in *Synechocystis*.

MATERIALS AND METHODS

Site-Directed Mutagenesis. The $Atx1^{ZiaA_N}$, $Atx1^{PacS_N}$, $PacS_N{}^{ZiaA_N}$, and $PacS_N{}^{Atx1}$ mutants (Figure 1C) were generated using QuikChange mutagenesis (Stratagene) with pETATX1 (encoding full length Atx1)[10] and pETPACS71 (encoding $PacS_N$, which constitutes the first 71 amino acids of PacS)[12] as templates and the primers given in Table S1 in the Supporting Information. Both strands of all DNA constructs were confirmed by sequencing.

Protein Purification, Reduction, Quantification, and Analysis. Proteins (including His61Tyr $Atx1^{12}$) were purified, reduced and quantified as previously reported,[12,14,23] and the $Atx1^{ZiaA_N}$, $Atx1^{PacS_N}$, $PacS_N{}^{ZiaA_N}$, and $PacS_N{}^{Atx1}$ variants were verified by mass spectrometry. Far-UV (185−250 nm) circular dichroism (CD) spectra[14] and analytical gel filtration chromatography[12] were performed as described previously. The dimerization constant (K_{dim}) for Cu(I)−$Atx1^{PacS_N}$ was determined by gel filtration as described previously.[12]

Zinc Titrations and the Determination of Zn(II) and Cu(I) Affinities. Titrations of Zn(II) into apo-proteins were performed in 25 mM 4-(2-hydroxyethyl)piperazine-1-ethanesulfonic acid (Hepes) pH 7.4 plus 100 mM NaCl and monitored for changes in absorbance at 240 nm on a λ35 UV/vis spectrophotometer (Perkin-Elmer).[14] Zn(II) affinities were measured using the competitive chelator RhodZin-3 in 25 mM Hepes pH 7.4 plus 100 mM NaCl.[14] Data were fit to a model (eq 1) considering a single species (ZnP, where P is the apo-protein) for $Atx1^{ZiaA_N}$ and $PacS_N{}^{ZiaA_N}$ to obtain the Zn(II) affinity of the apo-protein (K_{Zn}) and two species (ZnP and ZnP_2, see eq 2) for His61Tyr Atx1, $Atx1^{PacS_N}$, and $PacS_N{}^{Atx1}$ to determine both K_{Zn} and the affinity of the apo-protein for zinc-protein (K_{Zn2}). Below are eqs 1 and 2:

$$[P] = \frac{([Zn] - [ZnL])(K_b([L] - [ZnL]) + K_{Zn}[ZnL])}{K_{Zn}[ZnL]} \quad (1)$$

$$[P] = A\left(1 + \frac{[ZnL]K_{Zn}}{[L]K_b}\right) + \frac{2[ZnL]K_{Zn}K_{Zn2}}{[L]K_b}A^2 \quad (2)$$

where

$$A = \frac{-\frac{[ZnL]K_{Zn}}{[L]K_b} + \sqrt{\left(\frac{[ZnL]K_{Zn}}{[L]K_b}\right)^2 - \frac{4([ZnL] - [Zn])[ZnL]K_{Zn}K_{Zn2}}{[L]K_b}}}{\frac{2[ZnL]K_{Zn}K_{Zn2}}{[L]K_b}} \quad (3)$$

and where [L], [P] and [Zn] represent total RhodZin-3, protein, and zinc concentrations, respectively, and K_b is the zinc affinity of RhodZin-3.

For Cu(I) affinity (K_{Cu}) determinations, the chromophoric ligand bathocuproine disulfonate (BCS) was used in 20 mM Hepes pH 7.0 plus 200 mM NaCl. Data were fit to a 1:1 Cu(I):protein model (eqs 4 and 5),[14,23] except in the case of $Atx1^{PacS_N}$, for which data at multiple Cu(I) concentrations were fit to a model that also considers dimerization of the Cu(I)−protein (eq 6)[14] using a K_{dim} of 5.7×10^4 M^{-1} (vide infra). Below are eqs 4−6:

$$[L] = 2[CuL_2] + \sqrt{\frac{K_{Cu}([P] - [Cu] + [CuL_2])[CuL_2]}{\beta([Cu] - [CuL_2])}} \quad (4)$$

$$[P] = \frac{([Cu] - [CuL_2])([L] - 2[CuL_2])^2\beta}{K_{Cu}[CuL_2]} + [Cu] - [CuL_2] \quad (5)$$

$$[P] = [Cu] - [CuL_2] + \frac{\beta([L] - 2[CuL_2])^2}{4[CuL_2]K_{Cu}K_{dim}} \times (\sqrt{8K_{dim}([Cu] - [CuL_2]) + 1} - 1) \quad (6)$$

where [L], [P] and [Cu] represent total BCS, protein, and copper concentrations, respectively, and β is the formation constant of $[Cu(BCS)_2]^{3-}$.

Protein Crystallization, X-ray Data Collection, Structure Determination, and Refinement. $Atx1^{ZiaA_N}$ (25 mg/mL) loaded with 1 equiv of Zn(II) in 20 mM Hepes pH 7.0 and 100 mM NaCl was crystallized anaerobically from 1.6 M trisodium citrate pH 6.5 using the hanging drop method of vapor diffusion (1 μL protein and 0.5 mL well solution). $PacS_N{}^{ZiaA_N}$ (10 mg/mL) loaded with 1 equiv of Zn(II) in 20 mM Hepes pH 7.0 plus 35 mM NaCl was crystallized from 0.1 M Hepes pH 7.5 plus 10% (w/v) PEG 4000 and 5% (w/v) isopropanol (condition 1) using the sitting drop method (250 nL protein and 100 μL well solution). A second crystal form of

dx.doi.org/10.1021/bi400492t | *Biochemistry* 2013, 52, 6816−6823

Table 1. Crystallographic Data Collection and Processing Statistics

	Atx1^{ZiaA_N} Zn hrm[a]	Atx1^{ZiaA_N} Zn lrm[a]	PacS$_N^{ZiaA_N}$ [b] Zn hrm[a]	PacS$_N^{ZiaA_N}$ [b] Zn pk[a]	PacS$_N^{ZiaA_N}$ [c] Zn hrm[a]	PacS$_N^{ZiaA_N}$ [c] Zn pk[a]	PacS$_N^{ZiaA_N}$ [c] Zn lrm[a]
data collection							
instrumentation	Diamond I02		Diamond I02		Diamond I02		
wavelength (Å)	0.9795	1.3190	0.9795	1.2876	0.9795	1.2820	1.2876
space group	*H*32		$P2_1$		$P2_1$		
resolution range (Å)[d]	42.81−1.90 (2.00−1.90)	42.84−1.95 (2.09−1.95)	31.59−1.40 (1.48−1.40)	31.62−1.60 (1.68−1.60)	22.84−1.25 (1.32−1.25)	29.01−1.55 (1.63−1.55)	29.02−1.60 (1.68−1.60)
unit cell parameters (Å, deg)	a = 85.62	a = 85.68	a = 24.66	a = 24.69	a = 22.78	a = 22.78	a = 22.79
	b = 85.62	b = 85.68	b = 52.60	b = 52.62	b = 58.04	b = 58.02	b = 58.05
	c = 188.14	c = 188.48	c = 39.92	c = 39.96	c = 24.78	c = 24.77	c = 24.78
	α = 90.00	α = 90.00	α = 90.00	α = 90.00	α = 90.00	α = 90.00	α = 90.00
	β = 90.00	β = 90.00	β = 98.13	β = 98.08	β = 112.82	β = 112.81	β = 112.82
	λ = 188.14	λ = 120.00	λ = 90.00	λ = 90.00	λ = 90.00	λ = 90.00	λ = 90.00
unique reflections	21 226 (3053)	19 718 (2845)	18 146 (2491)	12 212 (1713)	15 818 (2012)	8459 (1167)	7835 (1133)
multiplicity[d,e]	5.7 (5.8)	5.6 (5.7)	4.0 (4.0)	4.0 (3.9)	3.3 (3.0)	3.3 (3.1)	3.4 (3.4)
[anomalous]	2.9 (3.0)	2.9 (2.9)	2.0 (2.0)	2.0 (1.9)	1.6 (1.6)	1.6 (1.6)	1.6 (1.6)
mean $(I/\sigma(I))$[d,e]	10.9 (4.1)	10.2 (2.9)	15.3 (5.1)	16.5 (3.6)	13.6 (4.2)	11.4 (4.3)	19.2 (7.3)
completeness (%)[d,e]	99.8 (100.0)	99.8 (100.0)	91.4 (86.2)	90.9 (87.8)	96.2 (87.5)	97.6 (91.0)	98.8 (99.4)
[anomalous]	99.8 (99.9)	99.8 (100.0)	84.3 (75.8)	82.9 (74.3)	90.8 (63.8)	93.1 (72.0)	96.8 (99.4)
R_{merge} (%)[d,e]	8.7 (37.4)	8.0 (43.7)	5.0 (22.1)	5.0 (38.4)	4.7 (25.5)	6.1 (19.9)	4.1 (15.9)

	Atx1^{ZiaA_N} Zn hrm	PacS$_N^{ZiaA_N}$ [b] Zn hrm	PacS$_N^{ZiaA_N}$ [c] Zn hrm
refinement			
resolution range (Å)[d]	42.81−1.90 (2.00−1.90)	31.59−1.40 (1.48−1.40)	22.84−1.25 (1.32−1.25)
TLS refinement	yes	no	no
anisotropic *B*-factors	no	yes	yes
R_{work} (%)[f]	19.47	13.98	14.29
R_{free} (%)[f]	24.30	19.53	17.99
rms bond (Å)[f]	0.0117	0.0109	0.0108
rms angles (deg)[f]	1.478	1.525	1.421
no. of non-hydrogen atoms	1919	1152	624
average *B*-factor (Å^2)			
protein	37.2	13.4	14.9
water	25.3	24.6	28.1
other solvent atoms	35.0	17.9	13.5
Ramachandran outliers	0	0	0
PDB accession codes	4A47	4A48	4A4J

[a]pk is data collected at the peak for the zinc edge, hrm is a high-energy remote data set, and lmr is a low-energy remote data set. [b]Condition 2. [c]Condition 1. [d]Figures in parentheses are those for the highest resolution shell, as given. [e]Reflection statistics are as reported by SCALA.[25] R_{merge} is calculated as described in SCALA.[25] [f]Refinement statistics are as reported by REFMAC5.[27,28]

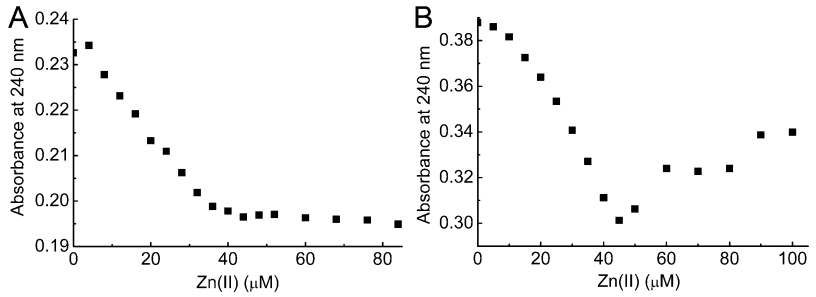

Figure 2. Plots of absorbance at 240 nm against Zn(II) concentration for apo-Atx1^{ZiaA_N} (A, 40 μM) and apo-PacS$_N^{ZiaA_N}$ (B, 50 μM) in 25 mM Hepes pH 7.4 plus 100 mM NaCl.

Zn(II)−PacS$_N^{ZiaA_N}$ was obtained from 20% (w/v) PEG 3350 plus 0.2 M NaF (condition 2). All crystals were frozen using *N*-paratone oil as the cryoprotectant. Diffraction data were collected at 100 K on beamline I02 at the Diamond Light Source (Didcot, U.K.). The identity of the metal was confirmed by calculation of an anomalous difference Fourier map using additional data sets collected both above [high-energy remote (hrm)] and below [low-energy remote (lrm)] the zinc K-edge

dx.doi.org/10.1021/bi400492t | *Biochemistry* 2013, 52, 6816−6823

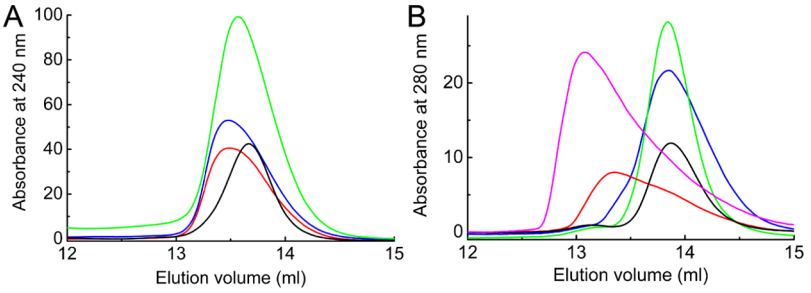

Figure 3. Plots of absorbance at 240 nm against elution volume from a gel filtration column for Atx1^{ZiaA_N} (A) and of absorbance at 280 nm against elution volume for PacS$_N^{ZiaA_N}$ (B). Data were acquired in 25 mM Tris pH 7.5 plus 200 mM NaCl. Data shown for apo-protein (blue line), protein loaded with 1 equiv of Cu(I) (green line), and protein with 0.5 (red line, also magenta line for PacS$_N^{ZiaA_N}$) and 1 (black line) equiv of Zn(II) at the loaded protein concentrations given in Table S3 in the Supporting Information [PacS$_N^{ZiaA_N}$ with 0.5 equiv of Zn(II) was loaded at 50 (red line) and 150 (magenta line) μM].

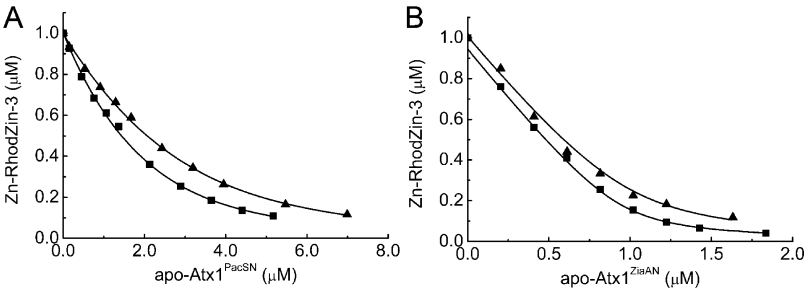

Figure 4. Titrations of Zn−RhodZin-3 (1 μM) and (A) excess RhodZin-3 [4 (■) and 9 (▲) μM] with apo-Atx1^{PacS_N} and (B) excess RhodZin-3 [19 (■) and 39 (▲) μM] with apo-Atx1^{ZiaA_N} in 25 mM Hepes pH 7.4 plus 100 mM NaCl. The simultaneous fit of the data for Atx1^{PacS_N} to eq 2 gives a K_{Zn} of (2.5 ± 0.1) × 10^8 M^{-1} and K_{Zn2} of (3.6 ± 0.4) × 10^5 M^{-1} and for Atx1^{ZiaA_N} to eq 1 gives a K_{Zn} of (2.5 ± 0.1) × 10^{10} M^{-1}.

(peak) to confirm the presence and absence, respectively, of the anomalous signal (Table 1). Data were processed and integrated using iMOSFLM and scaled with Scala.[24,25] The structures were solved by molecular replacement using Molrep[26] and 2XMT (Atx1) and 2XMW (PacS$_N$) as the search models.[12] Final models were produced with iterative cycles of refinement (Refmac5) and model-building using COOT.[27,28]

RESULTS AND DISCUSSION

Protein Purification and Characterization. Mass spectra (Table S2 in the Supporting Information) show that Atx1^{ZiaA_N}, PacS$_N^{Atx1}$, and PacS$_N^{ZiaA_N}$ are purified without their N-terminal Met residue. Atx1^{PacS_N} is isolated as a mixture of full length protein and protein missing Met1 (Table S2 in the Supporting Information). CD spectra (Figure S1 in the Supporting Information) demonstrate fully folded proteins and domains in all cases.

Oligomerization State of the Apo and Metal-Loaded Proteins. For most proteins studied, the addition of Zn(II) causes a decrease in absorbance at 240 nm (Figure 2 and Figure S2 in the Supporting Information) in the UV/vis spectrum [the absorbance at 240 nm does initially increase upon the addition of Zn(II) to apo-PacS$_N^{Atx1}$ (Supporting Information Figure S2B)]. This seems counterintuitive considering that the formation of Zn(II)−S bonds is normally accompanied by an increase in absorbance at this wavelength due to the appearance of S(Cys)→Zn(II) ligand to metal charge transfer bands.[29] However, a number of factors can give rise to changes in absorbance at 240 nm, including the protonation state of the Cys ligands, and the observed effects are probably the result of several contributing factors. Regardless of the absolute values, the change in absorbance at this wavelength upon Zn(II) addition does give insight into the stoichiometry of the complexes formed. The Zn(II) titrations (Figure 2 and Figure S2 in the Supporting Information) show an inflection point at ∼0.5 equiv, followed by a plateau after 1 equiv, for all proteins except Atx1^{ZiaA_N}, for which the decrease in absorbance at 240 nm is linear up to 1 equiv (Figure 2A). These data indicate the formation of a single Zn(II)-form (ZnP) for Atx1^{ZiaA_N}, as previously seen for ZiaA$_N$,[14] and two Zn(II)-loaded species (ZnP and ZnP$_2$) for PacS$_N^{ZiaA_N}$, His61Tyr Atx1, Atx1^{PacS_N}, and PacS$_N^{Atx1}$, as found for wild type (WT) Atx1 and PacS$_N$.[14] Consistent with this, most of these proteins elute as dimers from a gel filtration column when loaded with 0.5 equiv of Zn(II) (Figure 3 and Figure S3 and Table S3 in the Supporting Information), whereas Atx1^{ZiaA_N} elutes as a monomer, most probably as a mixture of apo- and Zn(II)-protein (Figure 3A and Table S3 in the Supporting Information). The elution volume of PacS$_N^{ZiaA_N}$ loaded with 0.5 equiv of Zn(II) decreases (apparent molecular weight increases) with increasing protein concentration, consistent with a relatively weak ZnP$_2$ dimer (Figure 3B and Table S3 in the Supporting Information). Atx1^{ZiaA_N} and PacS$_N^{ZiaA_N}$ elute as monomers when loaded with 1 equiv of Zn(II) (Figure 3A,B and Table S3 in the Supporting Information). All of the other proteins have a greater tendency to dimerize at the relatively high protein concentrations used for the gel filtration experiments (90−200 μM) and are recovered with approximately 0.5 Zn(II) equiv (Figure S3 and Table S3 in the Supporting Information).

We have previously shown that although WT apo-Atx1 is a monomer, when the protein is loaded with 1 equiv of Cu(I) [Cu(I)−Atx1], it elutes from a gel filtration column as a dimer. However, the elution volume increases upon lowering the

dx.doi.org/10.1021/bi400492t | Biochemistry 2013, 52, 6816−6823

Table 2. Cu(I) and Zn(II) Affinities (K_{Cu} and K_{Zn} Values, Respectively) and Affinities of the Apo-Protein for the Zn(II)-Protein (K_{Zn2} Values)[a]

	Cu(I)	Zn(II)	
protein	K_{Cu} (M^{-1})	K_{Zn} (M^{-1})	K_{Zn2} (M^{-1})
WT Atx1[b]	$(4.7 \pm 0.7) \times 10^{17}$ [c]	$(7.2 \pm 0.3) \times 10^{8}$	$(1.5 \pm 0.2) \times 10^{5}$
His61Tyr Atx1	$(1.8 \pm 0.3) \times 10^{17}$ [b]	$(2.8 \pm 0.3) \times 10^{8}$	$(1.9 \pm 0.4) \times 10^{5}$
$Atx1^{PacS_N}$	$(5.6 \pm 0.1) \times 10^{17}$ [c]	$(2.5 \pm 0.1) \times 10^{8}$	$(3.6 \pm 0.4) \times 10^{5}$
$Atx1^{ZiaA_N}$	$(1.4 \pm 0.5) \times 10^{17}$	$(2.5 \pm 0.1) \times 10^{10}$	
WT $PacS_N$[b]	$(7.8 \pm 0.7) \times 10^{16}$	$(4.2 \pm 0.4) \times 10^{7}$	$(2.6 \pm 0.3) \times 10^{5}$
$PacS_N^{Atx1}$	$(1.3 \pm 0.2) \times 10^{17}$	$(5.2 \pm 1.0) \times 10^{7}$	$(8.7 \pm 2.3) \times 10^{5}$
$PacS_N^{ZiaA_N}$	$(8.5 \pm 1.5) \times 10^{16}$	$(1.7 \pm 0.2) \times 10^{9}$	
$ZiaA_N$[b]	$(6.5 \pm 1.0) \times 10^{16}$	$(1.1 \pm 0.1) \times 10^{10}$	

[a]Cu(I) affinities were determined in 20 mM Hepes pH 7.0 plus 200 mM NaCl, and Zn(II) affinities were determined in 25 mM Hepes pH 7.4 plus 100 mM NaCl. [b]From ref 14. [c]Values for the monomeric protein determined from titrating apo-protein into $[Cu(BCS)_2]^{3-}$ at multiple Cu(I) concentrations.

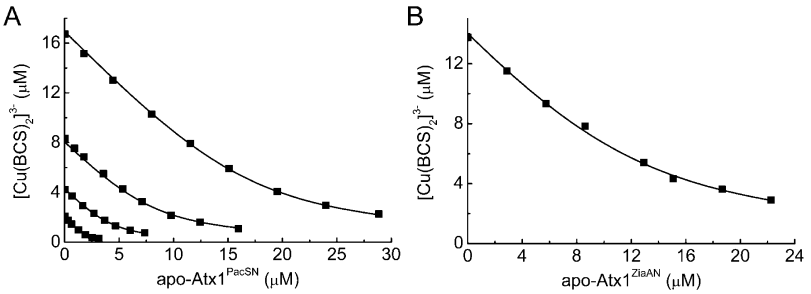

Figure 5. Titration of $[Cu(BCS)_2]^{3-}$ with apo-$Atx1^{PacS_N}$ (A) and apo-$Atx1^{ZiaA_N}$ (B) in 20 mM Hepes pH 7.0 plus 200 mM NaCl. In (A), the $[Cu(BCS)_2]^{3-}$ concentration ranges from 2.0 to 16.0 μM in the presence of an excess of BCS (46–168 μM). In (B), the $[Cu(BCS)_2]^{3-}$ concentration is 14.0 μM with an excess of BCS (72 μM) present. The fit of the data in (A) to eq 6 using a dimerization constant (K_{dim}) of 5.7×10^4 M^{-1} gives a K_{Cu} of $(5.6 \pm 0.1) \times 10^{17}$ M^{-1}, and the fit of the data in (B) to eq 5 gives a K_{Cu} of $(1.8 \pm 0.1) \times 10^{17}$ M^{-1}.

protein concentration below 100 μM, indicative of dimer dissociation in this concentration range, and an equilibrium constant (K_{dim}) of $(5 \pm 2) \times 10^5$ M^{-1} has been determined.[12] The mutation of His61 into a Tyr, the residue in the corresponding position on loop 5 in $PacS_N$ and $ZiaA_N$ (Figure 1), results in monomeric Cu(I)–Atx1 and a His residue at this key location, whose side chain hydrogen bonds with the Cys ligands (Figure 1), favors dimerization. All of the apo-variants loaded with 1 equiv of Cu(I) elute as monomers on a gel-filtration column (Figure 3 and Figure S3 and Table S3 in the Supporting Information) except for Cu(I)–$Atx1^{PacS_N}$, which elutes as a dimer (Figure S3A and Table S3 in the Supporting Information). A dimerization constant of $(6 \pm 1) \times 10^4$ M^{-1} was determined for Cu(I)–$Atx1^{PacS_N}$ (Figure S4 in the Supporting Information), ~10-fold lower than that of WT Atx1.[12] This lowered dimerization constant for $Atx1^{PacS_N}$ and the absence of dimer formation for $Atx1^{ZiaA_N}$ demonstrate that residues in the native IACEAC motif of Atx1 contribute to the stability of the dimer formed in the presence of Cu(I).

Zinc(II) and Copper(I) Affinities. Introducing the metal-binding motif of Atx1 into $PacS_N$ has almost no effect on Zn(II) affinity (K_{Zn}), whereas replacing the sequence of Atx1 with that of $PacS_N$ decreases the Zn(II) affinity 3-fold (Figure 4A and Table 2). The His61Tyr Atx1 mutation decreases the Zn(II) affinity by a similar amount (Table 2), and this loop 5 residue is therefore not involved in Zn(II) binding. The affinity of apo-protein for Zn(II)-protein (K_{Zn2}) is enhanced 2- to 3-fold in $Atx1^{PacS_N}$ and $PacS_N^{Atx1}$ but is almost unaltered by the His61Tyr Atx1 mutation (Table 2). The largest changes in Zn(II) affinity (up to 40-fold) result from introducing the $ZiaA_N$ sequence into $PacS_N$ and Atx1 (Figure 4B and Table 2). $Atx1^{ZiaA_N}$ has the highest Zn(II) affinity of all the proteins studied, ~2- and 15-fold tighter than those of $ZiaA_N$ and $PacS_N^{ZiaA_N}$, respectively (Table 2).

The Cu(I) affinity (K_{Cu}) of monomeric WT Atx1 is approximately an order of magnitude greater than those of WT $PacS_N$ and $ZiaA_N$ at pH 7 (Table 2).[14] Some of this difference is due to the presence of His61 on loop 5 of Atx1 because replacement with a Tyr, the residue found in this position in both $PacS_N$ and $ZiaA_N$, results in a ~2.5-fold decrease in Cu(I) affinity (Table 2).[14] The introduction of the metal-binding motif of $PacS_N$ has almost no effect on Cu(I) affinity of Atx1, but K_{Cu} decreases ~2- to 3-fold in $Atx1^{ZiaA_N}$ (Figure 5 and Table 2). The introduction of the Atx1 loop into $PacS_N$ (in $PacS_N^{Atx1}$) does increase the Cu(I) affinity ~3-fold (Table 2), whereas the Cu(I) affinity of $PacS_N^{ZiaA_N}$ is very similar to that of $PacS_N$ (Table 2). The non-Cys residues in the loop can influence the Cu(I) affinity by a similar amount as that seen upon mutating the loop 5 residue. These mutations all change the second-coordination sphere, which has a small effect on the Cu(I) affinity of copper-trafficking proteins, with the most important contribution being from residues that can influence the pK_a values of the Cys ligands.[23,30]

Crystal Structures of Zn(II)–$Atx1^{ZiaA_N}$ and Zn(II)–$PacS_N^{ZiaA_N}$. To gain insight into the structural causes of the large changes in Zn(II) affinity, Zn(II)–$Atx1^{ZiaA_N}$ and Zn(II)–$PacS_N^{ZiaA_N}$ have been crystallized. $Atx1^{ZiaA_N}$ loaded with 1 equiv of Zn(II) crystallizes as a Zn(II)-bridged dimer (Figure 6), an arrangement that is probably relevant for all the ZnP_2 forms that we have observed in solution (Table S3 in the Supporting Information). This arrangement (contact area ~450 Å^2) is remarkably similar to that of the side-to-side $Cu(I)_2$–Atx1

dx.doi.org/10.1021/bi400492t | Biochemistry 2013, 52, 6816–6823

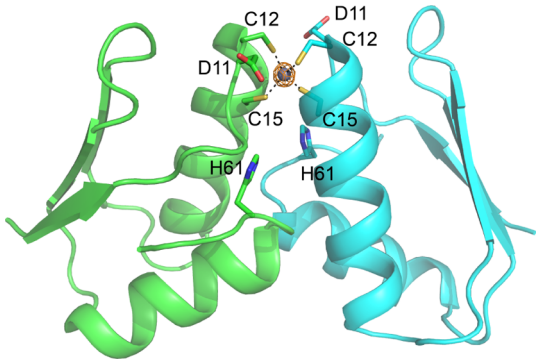

Figure 6. Structure of Zn(II)−Atx1^{ZiaA_N} showing the Zn(II) site at the dimer interface. The introduced Asp11 residue is not involved in coordinating Zn(II) but makes an intermolecular hydrogen bond with Ser14 (not shown). The zinc ion is shown as a gray sphere with the anomalous density (orange mesh) contoured at 12σ.

dimer[12] (rmsd for C^{α} atoms of ∼0.6 Å for each of the two monomers) even though the tetranuclear Cu(I) cluster is replaced by a single Zn(II) ion. This dimer is also very similar to that observed for WT Zn(II)−Atx1,[31] though some of the monomer-monomer interactions are different [oligomeric (mainly dimeric) forms are commonly observed in crystal structures of metalated forms of this Atx1[12,31]]. The Zn(II) site in the Atx1^{ZiaA_N} dimer is coordinated by Cys12 and Cys15 from each monomer in a tetrahedral arrangement, with Zn(II)−S^{γ} distances of ∼2.3−2.4 Å and S^{γ}−Zn−S^{γ} angles of 101−121°. The $O^{\delta 2}$ atom of Asp11 on the mutated motif is involved in an intermolecular hydrogen bond with Ser14 (O^{γ}), also from the mutated region. A further intermolecular hydrogen bond is present between Asn25 ($N^{\delta 2}$) and Ala57 (CO) as in the $[Cu(I)_2$−Atx1$]_2$ structure. The dimer arrangement of Zn(II)−Atx1^{ZiaA_N}, with monomers linked by a single metal ion, is also similar to those seen in crystal structures of metal-bound forms [Cu(I), Hg(II), Cd(II), or Pt(II)] of human Atx1 (HAH1).[17,32]

Different metal site structures are found in two crystal forms of Zn(II)−PacS$_N^{ZiaA_N}$ (Figure 7). In crystals obtained from

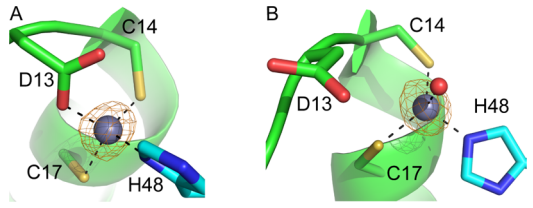

Figure 7. Structures of the Zn(II) sites in the two different crystal forms of Zn(II)−PacS$_N^{ZiaA_N}$. The monodentate carboxylate ligand in (A) is replaced by a water ligand in (B), and Asp13 has moved away from the Zn(II) ion. The anomalous density for zinc is shown (orange mesh) contoured at 5σ.

condition 1 (a monomer in the asymmetric unit), Zn(II) is bound by Cys14 and Cys17 from the MDCTSC motif with Zn(II)−S^{γ} distances of ∼2.3 Å. Coordination is completed by Asp13 (monodentate) from the same chain, as well as by His48 from an adjacent monomer, with Zn(II)−$O^{\delta 2}$ and Zn(II)−$N^{\delta 1}$ distances of 1.95 and 2.05 Å, respectively (Figure 7A). The bond angles range from 104 to 120°, consistent with tetrahedral coordination.

In the alternate crystal form (condition 2), the asymmetric unit contains a dimer with the monomer-monomer interface distal from the metal site. Zn(II)−PacS$_N^{ZiaA_N}$ is a monomer in solution (Figure 3B and Table S3 in the Supporting Information), and this crystallographic dimer is therefore an artifact. The metal site structure in this form of Zn(II)−PacS$_N^{ZiaAN}$is similar to that found in the condition 1 crystal structure except that Asp13 is replaced by a water ligand with a Zn(II)−O distance of ∼2.1 Å (Figure 7B). The carboxylate group of Asp13 points away from the metal site, is solvent exposed, and is not involved in any interactions.

Attempts to crystallize ZiaA$_N$ have been unsuccessful, and NMR studies could not determine the structure of the high affinity Zn(II) site.[13] NMR has also been used to investigate the MBD of the related Zn(II)-exporting ATPase from *E. coli* (ZntA).[18] In this case a $(Cys)_2$Asp Zn(II) site has been suggested, but because of the limitations of NMR data, neither the precise Zn(II) coordination number nor the geometry of the site could be resolved. This NMR study also suggested the possibility of a water ligand completing the coordination environment because of the solvent exposure of the Zn(II) site. Surprisingly, a recent NMR study of cyclic peptides that mimic Cu(I)- and Zn(II)-binding CXXC motifs (MTCSGCSRPG and MDCSGCSRPG, respectively) has found that the Asp residue (underlined) coordinates Cu(I) but not Zn(II).[33] The crystal structures of Zn(II)−PacS$_N^{ZiaA_N}$ are the first of a Zn(II) site bound by a CXXC motif involved in zinc transport. These structures provide strong evidence that the Asp residue preceding the CXXC motif binds Zn(II) in a monodentate fashion and that a water ligand can occupy the fourth coordination position of a tetrahedral site in the MBDs of Zn(II)-transporting proteins.

Insight into Zn(II) Trafficking Provided by the M/IXCXXC Motif Variants. The sequence of the metal-binding motif has a much more significant influence on Zn(II) than Cu(I) affinities, and introducing the ZiaA$_N$ sequence into Atx1 and PacS$_N$ increases the Zn(II) affinity by up to ∼40-fold. This is due to the side chain of Asp13 coordinating Zn(II), as seen in a Zn(II)−PacS$_N^{ZiaA_N}$ crystal structure (Figure 7A), which must also be the cause of the higher Zn(II) affinity of ZiaA$_N$. The two crystal forms of PacS$_N^{ZiaA_N}$ have Zn(II) sites with Cys_2His coordination, with either the carboxylate of Asp13 or a water molecule as the fourth ligand. A carboxylate group has a lower affinity for Zn(II) than Cys and His,[34] consistent with replacement of Asp13 and not the other ligands by water. The coordination of Zn(II) by Asp18 in ZiaA$_N$ tunes its Zn(II) affinity so that it is tighter than those of the Cu(I)-trafficking proteins (with two Cys ligands) but below that of the Zn(II) sensor (His_2Asp_2 coordination for SmtB from the cyanobacterium *Synechococcus*).[35,36] It has been suggested that Asp18 prevents ZiaA$_N$ from forming a stable complex with Cu(I)−Atx1.[37] A negatively charged residue close to the CXXC motif appears to be conserved in ATPases for metals (divalent) other than copper, and repulsion has been suggested as a common mechanism to prevent the binding of Cu(I). The presence of an Asp adjacent to the first Cys of the CXXC motif has almost no effect on Cu(I) affinity, as it is not required for coordination but is important for Zn(II) binding. With Zn(II) bound to ZiaA$_N$, the negative charge of Asp13 will no longer contribute to repulsing Atx1. As observed in our crystal structures, this Asp can readily dissociate, which may occur as Zn(II) is subsequently trafficked, allowing the negative charge to help prevent unwanted interactions (vide infra). The increase in Zn(II) affinity due to the introduction of an additional Zn(II) ligand appears to be sufficient to allow the MBDs of zinc and

dx.doi.org/10.1021/bi400492t | *Biochemistry* 2013, 52, 6816−6823

copper transporters that have very similar structures[12,13] to discriminate between these metals. It is therefore likely that the Zn(II) affinity of $ZiaA_N$ (10^{-10} M) is in the range of physiological free zinc concentrations in *Synechocystis*, although this has not been determined. This is supported by the observation that in *E. coli* up-regulation of ZntA expression occurs at nanomolar levels of intracellular free Zn(II),[38] which matches the Zn(II) affinities of both the MBD and the transmembrane site of ZntA ($\sim 10^8$ M^{-1}).[39]

The His residue (His48) involved in Zn(II) coordination in the $PacS_N^{ZiaA_N}$ structures belongs to an adjacent molecule. The recruitment of this His ligand only occurs at the high protein concentrations required for crystallization [Zn(II)−$PacS_N^{ZiaA_N}$ is monomeric in dilute solution (Figure 3B and Table S3 in the Supporting Information)] and is probably replaced by a water ligand in solution. However, in $ZiaA_N$, His residues from the unstructured C-terminus interact in solution with Zn(II) bound to the CXXC site.[13] These interactions were proposed to either aid metal transfer or alter intramolecular interactions. The observation that the side chain of Asp13 can be replaced by water when a His ligand is present highlights the fluxionality of this Zn(II) site, which will assist Zn(II)-trafficking. Our structures suggest two possible intermediates involving one of the His residues from the unstructured region of $ZiaA_N$, which could be important for zinc transfer. The coordination of Zn(II) by two His residues from the C-terminal region of $ZiaA_N$ (as well as by two Cys residues) would result in loss of the Asp ligand, enabling it to maintain a repulsive interaction with Atx1, to potentially hinder Cu(I) binding.

When the CXXC site of Atx1 binds 1 equiv of Zn(II), an exposed Zn(II) site with $Cys_2(H_2O)_2$ coordination will be present, which will be susceptible to ligand exchange reactions. This form may play a role in Zn(II) trafficking as it has been suggested that Atx1 can bind zinc in *Synechocystis*.[16] The unsaturated nature of such a Zn(II) site also makes it prone to coordinating additional ligands, such as Asp18 in $ZiaA_N$. Two additional Cys ligands can also be recruited from a second protein molecule, as seen in the crystal structure of Zn(II)−$Atx1^{ZiaA_N}$ (Figure 6), and as indicated for other proteins in this work, and also WT Atx1,[14,31] by studies in solution (Figures 2 and 3, and Figures S2 and S3 and Table S3 in the Supporting Information). These tetrathiolate sites are reminiscent of Zn(II) structural sites,[7] and their buried nature suggests they have limited functionality for Zn(II) trafficking but may play a role in storing the metal. However, given the fact that these dimers are relatively weak, there is likely fast dimer-monomer exchange so that Zn(II) can be easily accessed for the supply of endogenous Zn(II)-binding proteins. We have recently shown[31] that heterodimers between partner proteins (e.g., Atx1 and $PacS_N$) are formed in the presence of Zn(II) and are more stable than the corresponding homodimers, and may have a role in regulating the activity of copper-transporting ATPases.

CONCLUSIONS

The Zn(II) affinity of the MBD of a cyanobacterial zinc transporter is greatly enhanced by the presence of an Asp in the metal-binding motif due to the ability of the carboxylate group of this residue to coordinate the metal. The Zn(II) site in the MBD seems highly fluxional, which must be important for trafficking this metal and for other potential roles that the ligands, and particularly the Asp residue, may need to perform. The residues in the M/IXCXXC metal-binding motif of copper and zinc trafficking proteins have little influence on Cu(I) affinity.

ASSOCIATED CONTENT

Supporting Information

Figures showing CD spectra, Zn(II) titrations, gel filtration profiles and the dependence on protein concentration of the gel filtration elution volume for Cu(I)−$Atx1^{PacS_N}$, and tables showing primers, mass analyses, and gel filtration data. This material is available free of charge via the Internet at http://pubs.acs.org.

Accession Codes

The coordinates and structure factors have been deposited in the Protein Data Bank under the accession codes 4A47, 4A48, and 484J.

AUTHOR INFORMATION

Corresponding Author

*C. Dennison. E-mail: christopher.dennison@ncl.ac.uk. Phone: +44-191-222-7127. Fax: +44-191-222-7424.

Funding

This work was supported by the Biotechnology and Biological Sciences Research Council (BBSRC) grant BB/E016529.

Notes

The authors declare no competing financial interest.

ACKNOWLEDGMENTS

We thank staff at the Diamond Light Source for help with data collection and Dr. Nicolas Vita for performing some preliminary experiments.

REFERENCES

(1) Turski, M. L., and Thiele, D. J. (2009) New roles for copper metabolism in cell proliferation, signaling and disease. *J. Biol. Chem. 284*, 717−721.

(2) Vallee, B. L., and Auld, D. S. (1990) Zinc coordination, function, and structure of zinc enzymes and other proteins. *Biochemistry 29*, 5647−5659.

(3) Finney, L. A., and O'Halloran, T. V. (2003) Transition metal speciation in the cell: insights from the chemistry of metal ion receptors. *Science 300*, 931−936.

(4) Huffman, D. L., and O'Halloran, T. V. (2001) Function, structure and mechanism of intracellular copper trafficking proteins. *Annu. Rev. Biochem. 70*, 677−701.

(5) Nies, D. H. (2007) How cells control zinc homeostasis. *Science 317*, 1695−1696.

(6) Krezel, A., and Maret, W. (2007) Dual nanomolar and picomolar Zn(II) binding properties of metallothionein. *J. Am. Chem. Soc. 129*, 10911−10921.

(7) Maret, W., and Li, Y. (2009) Coordination dynamics of zinc in proteins. *Chem. Rev. 109*, 4682−4707.

(8) Thelwell, C., Robinson, N. J., and Turner-Cavet, J. S. (1998) An SmtB-like repressor from *Synechocystis* PCC 6803 regulates a zinc exporter. *Proc. Natl. Acad. Sci. U. S. A. 95*, 10728−10733.

(9) Tottey, S., Rich, P. R., Rondet, S. A., and Robinson, N. J. (2001) Two Menkes-type ATPases supply copper for photosynthesis in *Synechocystis* PCC 6803. *J. Biol. Chem. 276*, 19999−20004.

(10) Tottey, S., Rondet, S. A., Borrelly, G. P., Robinson, P. J., Rich, P. R., and Robinson, N. J. (2002) A copper metallochaperone for photosynthesis and respiration reveals metal specific targets, interaction with an importer, and alternative sites for copper acquisition. *J. Biol. Chem. 277*, 5490−5497.

(11) Banci, L., Bertini, I., Ciofi-Baffoni, S., Su, X. C., Borrelly, G. P., and Robinson, N. J. (2004) Solution structures of a cyanobacterial

metallochaperone. Insight into an atypical copper-binding motif. *J. Biol. Chem. 279*, 27502−27510.
(12) Badarau, A., Firbank, S. J., McCarthy, A. A., Banfield, M. J., and Dennison, C. (2010) Visualizing the metal-binding versatility of copper trafficking sites. *Biochemistry 49*, 7798−7810.
(13) Banci, L., Bertini, I., Ciofi-Baffoni, S., Poggi, L., Vanarotti, M., Tottey, S., Waldron, K. J., and Robinson, N. J. (2010) NMR structural analysis of the soluble domain of ZiaA-ATPase and the basis of selective interactions with copper metallochaperone Atx1. *J. Biol. Inorg. Chem. 15*, 87−98.
(14) Badarau, A., and Dennison, C. (2011) Thermodynamics of copper and zinc distribution in the cyanobacterium *Synechocystis* PCC 6803. *Proc. Natl. Acad. Sci. U. S. A. 108*, 13007−13012.
(15) Rao, L., Cui, Q., and Xu, X. (2010) Electronic properties and desolvation penalties of metal ions plus protein electrostatics dictate the metal binding affinity and selectivity in the copper efflux regulator. *J. Am. Chem. Soc. 132*, 18092−18102.
(16) Dainty, S. J., Patterson, C. J., Waldron, K. J., and Robinson, N. J. (2010) Interaction between cyanobacterial copper chaperone Atx1 and zinc homeostasis. *J. Biol. Inorg. Chem. 15*, 77−85.
(17) Wernimont, A. K., Huffman, D. L., Lamb, A. L., O'Halloran, T. V., and Rosenzweig, A. C. (2000) Structural basis for copper transfer by the metallochaperone for the Menkes/Wilson disease proteins. *Nat. Struct. Biol. 7*, 766−771.
(18) Banci, L., Bertini, I., Ciofi-Baffoni, S., Finney, L. A., Outten, C. E., and O'Halloran, T. V. (2002) A new zinc-protein coordination site in intracellular metal trafficking: solution structure of the apo and Zn(II) forms of ZntA(46−118). *J. Mol. Biol. 323*, 883−897.
(19) Hussain, F., Olson, J. S., and Wittung-Stafshede, P. (2008) Conserved residues modulate copper release in human copper chaperone Atox1. *Proc. Natl. Acad. Sci. U. S. A. 105*, 11158−11163.
(20) Rodriguez-Granillo, A., and Wittung-Stafshede, P. J. (2008) Structure and dynamics of Cu(I) binding in copper chaperones Atox1 and CopZ: a computer simulation study. *Phys. Chem. B 112*, 4583−4593.
(21) Rodriguez-Granillo, A., and Wittung-Stafshede, P. (2009) Differential roles of Met10, Thr11, and Lys60 in structural dynamics of human copper chaperone Atox1. *Biochemistry 48*, 960−972.
(22) Rodriguez-Granillo, A., and Wittung-Stafshede, P. J. (2009) Tuning of copper-loop flexibility in *Bacillus subtilis* CopZ copper chaperone: role of conserved residues. *J. Phys. Chem. B 113*, 1919−1932.
(23) Badarau, A., and Dennison, C. (2011) Copper trafficking mechanism of CXXC-containing domains: insight from the pH-dependence of their Cu(I) Affinities. *J. Am. Chem. Soc. 133*, 2983−2988.
(24) Battye, T. G., Kontogiannis, L., Johnson, O., Powell, H. R., and Leslie, A. G. (2011) iMOSFLM: a new graphical interface for diffraction-image processing with MOSFLM. *Acta Crystallogr., Sect. D: Biol. Crystallogr. 67*, 271−281.
(25) Evans, P. (2006) Scaling and assessment of data quality. *Acta Crystallogr., Sect. D: Biol. Crystallogr. 62*, 72−82.
(26) Vagin, A., and Teplyakov, A. (2010) Molecular replacement with MOLREP. *Acta Crystallogr., Sect. D: Biol. Crystallogr. 66*, 22−25.
(27) Collaborative Computational Project Number 4 (1994) The CCP4 suite: programs for protein crystallography. *Acta Crystallogr., Sect. D: Biol. Crystallogr. 50*, 760−763.
(28) Emsley, P., Lohkamp, B., Scott, W. G., and Cowtan, K. (2010) Features and development of coot. *Acta Crystallogr., Sect. D: Biol. Crystallogr. 66*, 486−501.
(29) Vasak, M., Kagi, J. H., and Hill, H. A. (1981) Zinc(II), cadmium(II), and mercury(II) thiolate transitions in metallothionein. *Biochemistry 20*, 2852−2856.
(30) Allen, S., Badarau, A., and Dennison, C. (2013) The influence of protein folding on the copper affinities of trafficking and target sites. *Dalton Trans. 42*, 3233−3239.
(31) Badarau, A., Basle, A., Firbank, S. J., and Dennison, C. (2013) Crosstalk between Cu(I) and Zn(II) homeostasis via Atx1-like domains. *Chem. Commun. 49*, 8000−8002.
(32) Boal, A. K., and Rosenzweig, A. C. (2009) Crystal structures of cisplatin bound to a human copper chaperone. *J. Am. Chem. Soc. 131*, 14196−14197.
(33) Shoshan, M. S., Shalev, D. E., and Tshuva, E. Y. (2013) Peptide models of Cu(I) and Zn(II) metallochaperones: the effect of pH on coordination and mechanistic implications. *Inorg. Chem. 52*, 2993−3000.
(34) Trzaskowski, B., Adamowicz, L., and Deymier, P. A. (2008) A theoretical study of zinc(II) interactions with amino acid models and peptide fragments. *J. Biol. Inorg. Chem. 13*, 133−137.
(35) VanZile, M. L., Cosper, N. J., Scott, R. A., and Giedroc, D. P. (2000) The zinc metalloregulatory protein *Synechococcus* PCC7942 SmtB binds a single zinc ion per monomer with high affinity in a tetrahedral coordination geometry. *Biochemistry 39*, 11818−11829.
(36) Eicken, C., Pennella, M. A., Chen, X., Koshlap, K. M., VanZile, M. L., Sacchettini, J. C., and Giedroc, D. P. (2003) A metal-ligand-mediated intersubunit allosteric switch in related SmtB/ArsR zinc sensor proteins. *J. Mol. Biol. 333*, 683−695.
(37) Tottey, S., Patterson, C. J., Banci, L., Bertini, I., Felli, I. C., Pavelkova, A., Dainty, S. J., Pernil, R., Waldron, K. J., Foster, A. W., and Robinson, N. J. (2012) Cyanobacterial metallochaperone inhibits deleterious side reactions of copper. *Proc. Natl. Acad. Sci. U. S. A. 109*, 95−100.
(38) Wang, D., Hosteen, O., and Fierke, C. A. (2012) ZntR-mediated transcription of zntA responds to nanomolar intracellular free zinc. *J. Inorg. Biochem. 111*, 173−181.
(39) Liu, J., Dutta, S. J., Stemmler, A. J., and Mitra, B. (2006) Metal-binding affinity of the transmembrane site in ZntA: implications for metal selectivity. *Biochemistry 45*, 763−772.